Journal of Power Sources 184 (2008) 44–51

Contents lists available at ScienceDirect

Journal of Power Sources

journal homepage: www.elsevier.com/locate/jpowsour

Study of poly(vinyl alcohol)/titanium oxide composite polymer membranes and their application on alkaline direct alcohol fuel cell

Chun-Chen Yang[a,*], Shwu-Jer Chiu[a], Kuo-Tong Lee[a], Wen-Chen Chien[a], Che-Tseng Lin[a], Ching-An Huang[b]

[a] Department of Chemical Engineering, Mingchi University of Technology, Taipei Hsien 243, Taiwan, ROC
[b] Department of Mechanical Engineering, Chang Guang University, Taoyuan 333, Taiwan, ROC

ARTICLE INFO

Article history:
Received 5 March 2008
Received in revised form 14 May 2008
Accepted 6 June 2008
Available online 14 June 2008

Keywords:
PVA/TiO_2
Composite polymer membrane
Direct alcohol fuel cell (DAFC)
Alkaline
MnO_2/BP2000

ABSTRACT

The novel poly(vinyl alcohol)/titanium oxide (PVA/TiO_2) composite polymer membrane was prepared using a solution casting method. The characteristic properties of the PVA/TiO_2 composite polymer membrane were investigated by thermal gravimetric analysis (TGA), a scanning electron microscopy (SEM), a micro-Raman spectroscopy, a methanol permeability measurement and the AC impedance method. An alkaline direct alcohol (methanol, ethanol and isopropanol) fuel cell (DAFC), consisting of an air cathode based on MnO_2/C inks, an anode based on PtRu (1:1) black and a PVA/TiO_2 composite polymer membrane, was assembled and examined for the first time. The results indicate that the alkaline DAFC comprised of a cheap, non-perfluorinated PVA/TiO_2 composite polymer membrane shows an improved electrochemical performances. The maximum power densities of alkaline DAFCs with 4 M KOH + 2 M CH_3OH, 2 M C_2H_5OH and 2 M isopropanol (IPA) solutions at room temperature and ambient air are 9.25, 8.00, and 5.45 mW cm^{-2}, respectively. As a result, methanol shows the highest maximum power density among three alcohols. The PVA/TiO_2 composite polymer membrane with the permeability values in the order of 10^{-7} to 10^{-8} cm^2 s^{-1} is a potential candidate for use on alkaline DAFCs.

1. Introduction

Alcohols (methanol, ethanol, and isopropanol) are often used as fuels for direct alcohol fuel cells (DAFCs) [1–32]. DAFCs have recently gained a great deal of attention for their highly potential applications in terms of electric vehicles (EVs), stationary applications, and portable power sources, such as cellular phones and notebook computers, etc. At present, direct methanol fuel cells (DMFCs) [1–17] are being actively studied and a lot of progress has been made during the past few years. However, the development of DMFCs has been hampered due to several serious problems, including slow methanol oxidation kinetics and incomplete electrooxidation of methanol, the poisoning of adsorbed intermediate species on the Pt surface, the high methanol crossover through the solid-state polymer Nafion membrane, and the high costs of the Nafion polymer membrane and Pt catalyst.

Aside from methanol, ethanol is much safer and can be produced in great quantities by fermentation of sugar-containing materials. Recently, direct ethanol fuel cells (DEFCs) [18–30] have also received a lot of attention due to these power sources possessing a high energy density and low emitting of pollutants. It is because ethanol is a green fuel, which simplifies the problems of delivery and storage and their high theoretical mass energy density (7.4 kW h kg^{-1}). Moreover, a liquid fuel can be used at ambient temperatures and pressures; thus DEFCs have the potential to be used on low-temperature fuel cells. However, the development of DEFCs has also faced several obstacles, including poor performance of the anode catalysts, the poisoning of the air cathode due to various adsorbed intermediate species on the catalyst surface, high ethanol crossover through the Nafion polymer membrane, and the high cost of a fully perfluorinated Nafion membrane and the Pt or Pt-alloy catalyst.

Recently, Yang [31,32] synthesized the crosslinked PVA composite polymer membrane applied to alkaline DMFCs. More precisely, the carbonation problem of alkaline DAFCs can be reduced by using an alkaline solid polymer membrane instead of an alkaline solution [5,33–35]. In addition, as we know, the anodic electrooxidation of alcohols in alkaline media shows much faster kinetics than that in acidic media [30].

Nanocrystalline titanium oxide (TiO_2, also called titania) has been extensively studied owing to its outstanding physical and chemical properties. Titania is usually used in the form of nanoparticles with high surface area, activity and excellent chemical stability. The addition of hydrophilic nanocrystalline titanium oxide

* Corresponding author. Tel.: +886 29089899; fax: +886 29041914.
E-mail address: ccyang@ccsun.mit.edu.tw (C.-C. Yang).

0378-7753/$ – see front matter © 2008 Elsevier B.V. All rights reserved.
doi:10.1016/j.jpowsour.2008.06.011

(TiO_2) filler into the polymer matrix serves to reduce the glass transition temperature (T_g) and the crystallinity of the PVA polymer and increase the amorphous phases of the polymer matrix, as well as increase its ionic conductivity. There are several ceramic fillers, such as TiO_2 [31], SiO_2 [35], that have been extensively studied. We know that when the TiO_2 filler used as a stiffer material is added to the PVA matrix, the swelling ratio of the PVA/TiO_2 composite polymer membrane is effectively reduced. Further, the thermal property, dimensional stability and long-term cycle life can also be improved.

In this paper, we attempted to disperse nano-sized TiO_2 ceramic fillers into the PVA matrix to act as a solid plasticizer capable of enhancing the chemical and thermal properties, as well as the dimension stability of the PVA/TiO_2 composite polymer membrane. Alkaline DAFCs, composed of the cathode loaded with MnO_2/BP2000 carbon ink on Ni-foam, the anode with PtRu (1:1) black on Ni-foam and the PVA/TiO_2 composite polymer membrane, were assembled and investigated. The PVA/TiO_2 composite polymer membrane was first prepared by blending the PVA polymer and nano-sized TiO_2 fillers while stirring. The solid composite polymer membrane was then immersed into a 5 wt.% glutaraldehyde (GA) solution for the crosslinking treatment. To allow for comparisons, three lower aliphatic alcohol fuels (C_1–C_3), i.e., methanol, ethanol and isopropanol, were individually tested. The electrochemical characteristics of the alkaline DAFCs comprised of the PVA/TiO_2 composite polymer membranes were studied following the linear polarization and galvanostatic methods, primarily to determine the peak power density of the alkaline DAFCs.

2. Experimental

2.1. Preparation of the PVA/TiO_2 composite polymer membrane

PVA (Aldrich), nanocrystalline TiO_2 fillers (anatase, 10–30 nm, 330 $m^2\,g^{-1}$, CBT, Taiwan), and KOH (Merck) were used as received without further purification. The degree of polymerization and saponification of PVA polymer were 1700 and 98–99%, respectively. The PVA/TiO_2 composite polymer membrane was prepared by using solution casting method. The appropriate quantities of PVA and TiO_2 in weight ratio 2–15% were kept under stirring in distilled water. The above resulting solution was stirred continuously until the solution mixture attained homogeneous viscous appearance at 95 °C for 2 h. The amounts of the TiO_2 fillers added and the blend time were well controlled. The resulting solution mixture was poured out on a glass plate. The thickness of the wet composite polymer membrane was between 0.020 and 0.040 cm. The glass plate with the viscous PVA/TiO_2 composite polymer sample was weighed again and then the excess water was allowed to evaporate slowly at 60 °C with a relative humidity of 30 RH%. After evaporation, the glass plate with the composite solid polymer membrane was weighed again. The composition of the PVA/TiO_2 composite polymer membrane was calculated from the mass balance. The thickness of the dried composite polymer membrane was controlled, remaining within a range of 0.010–0.020 cm. The dried PVA/TiO_2 composite polymer membrane was further crosslinked by immersing it in a 5 wt.% solution of glutaraldehyde (GA, 25 wt.% content in distilled water, Merck), 1.0 vol.% HCl, and acetone for the crosslinking reaction at 40 °C for 24 h.

2.2. Crystal structure, morphology, and thermal analyses

TGA thermal analysis was carried out using a PerkinElmer Pyris 7 TGA system. Measurements were carried out during heating from 25 to 500 °C, under N_2 atmosphere at a heating rate of 10 °C min^{-1} with an approximately 10 mg sample. The surface morphology and microstructure of the PVA/TiO_2 composite polymer membrane was investigated using a Hitachi S-2600H scanning electron microscope (SEM).

2.3. Ionic conductivity and methanol permeability measurements

Conductivity measurements were made for the alkaline PVA/TiO_2 composite polymer membranes using an AC impedance method. A 4 M KOH electrolyte solution was used rather than an 8 M KOH, due to the better alcohol solubility of a 4 M KOH solution. The PVA/TiO_2 composite samples were immersed in 4 M KOH solutions for 24 h before measurement. Alkaline PVA/TiO_2 composite polymer membranes were clamped between SS304 stainless steel, ion-blocking electrodes, each of surface area 1.32 cm^2, in a spring-loaded glass holder. A thermocouple was placed close to the composite polymer membrane to ensure correct temperature measurement. Each sample was equilibrated at the experimental temperature for at least 30 min before measurement. AC impedance measurements were carried out using Autolab PGSTAT-30 equipment (Eco Chemie B.V., the Netherlands). The AC spectra in the range of 300 kHz to 10 Hz at an excitation signal of 5 mV were recorded. AC impedance spectra of the composite polymer membrane were recorded at a temperature range between 30 and 70 °C. Experimental temperatures were maintained within ±0.5 °C using a convection oven. All PVA/TiO_2 composite polymer membranes were examined at least three times.

Alcohol permeability measurements [36,37] were conducted using a diffusion cell. The cell was divided into two compartments, in which one compartment was filled with D.I. water (called B compartment) and the other compartment filled with a 20 wt.% alcohol (methanol, ethanol, and IPA) aqueous solution (called A compartment). Prior to measurement, the PVA/TiO_2 composite polymer membrane was hydrated in D.I. water for at least 24 h. The composite polymer membrane with a surface area of 0.58 cm^2 was sandwiched between an O-ring and clamped tightly between the two compartments. The glass diffusion cell was continuously stirring during the experiment. The concentration of alcohol diffused from compartment A to B across the PVA/TiO_2 composite membrane was examined over time using a density meter (Mettler Toledo, DE45). Every 30 min, 0.20 mL was sampled from the B compartment. Before the permeation experiment, a calibration curve for the value of density vs. the alcohol concentration was prepared. The calibration curve was used to calculate the alcohol concentration in the permeation experiment. The alcohol permeability was calculated from the slope of the straight-line plot of alcohol concentration vs. permeation time. The alcohol concentration in the B compartment as a function of time is given in Eq. (1) [36,37]:

$$C_B(t) = \frac{A}{V}\frac{DK}{L}C_A(t - t_0) \quad (1)$$

where C is the alcohol concentration, A and L are the composite polymer membrane area and thickness; and D and K are the alcohol diffusivity and partition coefficient between the polymer membrane and the solution. The product DK is the polymer membrane permeability (P), t_0, also termed time lag, is related to the diffusivity: $t_0 = L^2/6D$.

2.4. Micro-Raman spectroscopy analyses

Micro-Raman spectrum is a simple tool to characterize the PVA/TiO_2 composite polymer membrane. Raman spectroscopy analysis was carried out using a Renishaw confocal microscopy Raman spectroscopy system with a microscope equipped with a 50× objective and a charge coupled device (CCD) detector. The Raman excitation source was provided by 632.8 nm He-Ne laser

beam with a beam power about 17 mW and was focused on the sample with a spot size of about 1 μm in diameter.

2.5. Preparation of the anode and cathode electrodes

The preparation of the catalyst slurry ink for the anode included mixing 70 wt.% PtRu black ink (Alfa, HiSPEC 6000, PtRu black with Pt:Ru = 1:1 at. ratio), 30 wt.% PTFE binder solution (Du Pont, 60 wt.% base solution), and a suitable amount of distilled water and alcohol. The resulting PtRu black mixtures were first ultrasonicated for 2 h. The PtRu black inks were then loaded onto Ni-foam using the impregnation method to achieve a loading of PtRu (1:1) black of 3.60 mg cm^{-2}. The as-prepared PtRu anode was dried in a vacuum oven at 110 °C for 2 h.

The carbon slurry for the gas diffusion layer of the air cathode was prepared using a mixture of 70 wt.% Shawinigan acetylene black (AB50) with a specific surface area of 80 m^2 g^{-1} and 30 wt.% PTFE solution (Teflon-30 suspension) as a wet-proofing agent and binder. The carbon slurry was coated on the Ni-foam used as a current collector and then pressed at 100 kg_f cm^{-2}. The gas diffusion layer was then sintered at temperature of 360 °C for 30 min. The catalyst layer of the air cathode was then prepared by spraying a mixture of a 15 wt.% of PTFE solution binder and 85 wt.% of mixed powders consisting of a MnO_2 catalyst mixed with BP2000 carbon black (MnO_2:BP2000 = 1:1). The Ni-foam with an area of 1 cm^2 was used as a current collector. The preparation methods of air electrodes have previously been reported in detail [38].

2.6. Electrochemical measurements

The PVA/TiO_2 composite polymer membrane was sandwiched between the sheets of the anode and the cathode, and then pressed at 25 °C at 120 kg_f cm^{-2} for 5 min to obtain a membrane electrode assembly (MEA). The electrode area of the MEA was about 1 cm^2.

The electrochemical measurements of the PtRu anode containing 3.6 mg cm^{-2} were carried out using a three-electrode system. The polarization curve of the PtRu anode and the air cathode was recorded at a scan rate of 1 mV s^{-1} at 25 °C. AC spectra of the PtRu anode with a frequency range of 100 kHz to 0.01 Hz at an excitation signal of 5 mV were examined at OCP. The electrochemical measurements for the DAFCs were also carried out using a two-electrode system. The *E*–*t*, *I*–*V*, and the power density curves of the alkaline DAFCs comprised of the PVA/TiO_2 composite polymer membrane were recorded at a current density of 20 mA cm^{-2} and at a scan rate of 1 mV s^{-1}, respectively. All electrochemical measurements were performed on an Autolab PGSTAT-30 electrochemical system with GPES 4.8 package software (Eco Chemie, the Netherlands). The electrochemical performances of the alkaline DAFC with the PVA/TiO_2 composite polymer membrane and the cathode open to atmospheric air were systematically studied in 4 M KOH + 2 M methanol, 2 M ethanol and 2 M IPA solutions, respectively, at room temperature and ambient air.

3. Results and discussion

3.1. TGA thermal analyses

Fig. 1 shows the TGA curves of the pure PVA film, the PVA/5 wt.% TiO_2 SPE, the 25 wt.% GA solution and the PVA/10 wt.% TiO_2 + 5 wt.% GA SPE, respectively. The TGA curve of the pure PVA film shows three major weight loss regions. The first region occurred at a temperature of 80–100 °C ($T_{max,1}$ = 100 °C) due to the evaporation of free and bound water; the weight loss of the membrane was about 3–4 wt.%. The second transition region occurred at around 260–340 °C ($T_{max,2}$ = 284 °C) due to the degradation of the PVA polymer film; the total weight loss at this stage was about 65–70 wt.%. The peak of the third stage at around 410–430 °C ($T_{max,3}$ = 428 °C) was due to the cleavage backbone of the PVA polymer film; the total weight loss was ca. 92 wt.% at 500 °C.

Fig. 1 also illustrates the TGA curves of the PVA + 5 wt.% GA SPE and the GA solution, respectively. The TGA curve of the PVA + 5 wt.% GA SPE membrane shows four major weight loss regions; however, the GA (25 wt.%) solution only shows two major weight loss regions. For the PVA + 5 wt.% GA film, the first region at a temperature of 80–100 °C ($T_{max,1}$ = 100 °C) was due to the evaporation of free and bound water; the weight loss of the membrane was also about 4–6 wt.%. The second transition region at around 140–190 °C ($T_{max,2}$ = 180 °C) was due to the degradation of the glutaraldehyde (GA) crosslinker; the total weight loss at this stage corresponded to about 15–20 wt.%. The peak of the third stage at around 300–340 °C ($T_{max,3}$ = 332 °C) was due to the degradation of PVA polymer membrane. The peak of the fourth stage at 410–440 °C ($T_{max,4}$ = 433 °C) was due to the cleavage of the C–C backbone of PVA polymer membranes; the total weight loss was about 85–90 wt.% at 500 °C.

The thermal property of the GA solution was also examined by TGA for comparison. As shown in Fig. 1, the first region at a temperature of 30–100 °C ($T_{max,1}$ = 90 °C) was due to the evaporation of free and bound water; the weight loss of the membrane was also about 80–90 wt.%. The second transition region at around 100–190 °C ($T_{max,2}$ = 180 °C) was due to the degradation of the glutaraldehyde (GA); the total weight loss at this stage corresponded to about 5–6 wt.%.

Moreover, the TGA curve of the PVA/10 wt.% TiO_2 + 5 wt.% GA SPE shows four major weight loss regions, which appear as four peaks in the DTG curves (not shown). The first region at a temperature of 80–100 °C ($T_{max,1}$ = 100 °C) was also due to the evaporation of free and bound H_2O; the weight loss of the membrane was 4–5 wt.%. The second transition region at around 130–190 °C ($T_{max,2}$ = 180 °C) was due to the degradation of the GA crosslinker; the total weight loss at this stage corresponded to about 15–20 wt.%. The peak of the third stage at around 350–380 °C ($T_{max,3}$ = 364 °C) was also due to

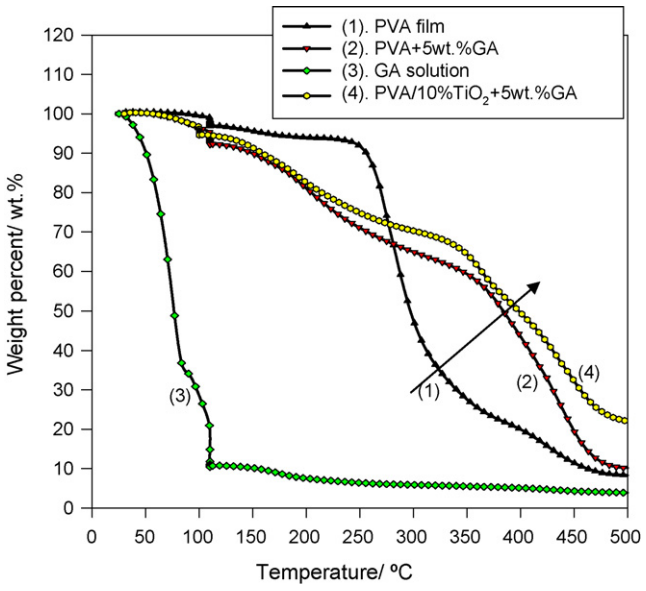

Fig. 1. TGA curves for PVA film, PVA + GA film, GA solution, and PVA/10% TiO_2 + 5 wt.% GA composite polymer membrane.

the degradation of PVA polymer membrane. The peak of the fourth stage at 420–480 °C ($T_{max,4}$ = 444 °C) was due to the cleavage C–C backbone of PVA polymer membrane; the total weight loss is ca. 78–80 wt.% at 500 °C.

Overall, the degradation peaks of the crosslinked PVA/TiO_2 composite polymer samples were less intense and shifted towards higher temperatures. It can be seen that the improved thermal stability was probably due to the additive effect of TiO_2 fillers and the chemical cross-link reaction between PVA and GA.

3.2. Surface morphology and micro-Raman analyses

An SEM photograph of the surface morphology for the PVA/5 wt.% TiO_2 composite polymer membrane is shown in Fig. 2, at a magnification of 2500×. The surface morphology of the PVA/TiO_2 composite polymer sample shows many aggregates or chunks randomly distributed on the top surface. It was found that the dimension of those TiO_2 aggregates embedded in the PVA matrix were around 5–200 μm. The results indicate that the nano-sized TiO_2 particles tended to form aggregates and dispersed into the PVA polymer matrix.

However, the hydrophilic PVA polymer and the TiO_2 fillers proved homogeneous and compatible without any phase separation occurring when a suitable amount of TiO_2 ceramic fillers was added. In summary, a suitable amount of TiO_2 fillers (as an alcohol permeation barrier) in the polymer network matrix [34,35] may assist in reducing alcohol crossover through the solid composite polymer membrane.

Fig. 3(a) shows the micro-Raman spectra of PVA powders and pure PVA polymer film, both of which showed several strong characteristic scattering peaks for the PVA polymer at 1440, 1383, 917 and 854 cm^{-1}, respectively. Fig. 3(b) shows the micro-Raman spectra of the TiO_2 powders (anatase), pure PVA film, and PVA/5 wt.% TiO_2 composite polymer membrane, respectively. It can be seen from micro-Raman spectra that the strong characteristic scattering peaks of TiO_2 fillers at 145, 194, 398, 517 and 638 cm^{-1} were for O–Ti–O, and they were due to the Ti–O bending and stretching vibrations. By contrast, a strong peak for the PVA polymer at 1440 cm^{-1} was due to the C–H bending and O–H bending. Moreover, the two additional vibrational peaks for the PVA polymer at 912 and 851 cm^{-1} were due to the C–C stretching. Additionally, there were several weak scattering peaks at 1146, 1093 and 1066 cm^{-1} [34]; they were due to the C–C stretching and C–O stretching, as also shown in Fig. 3(a). The assignment and frequency for major Raman peaks for the PVA polymer and TiO_2 powders are listed in Table 1.

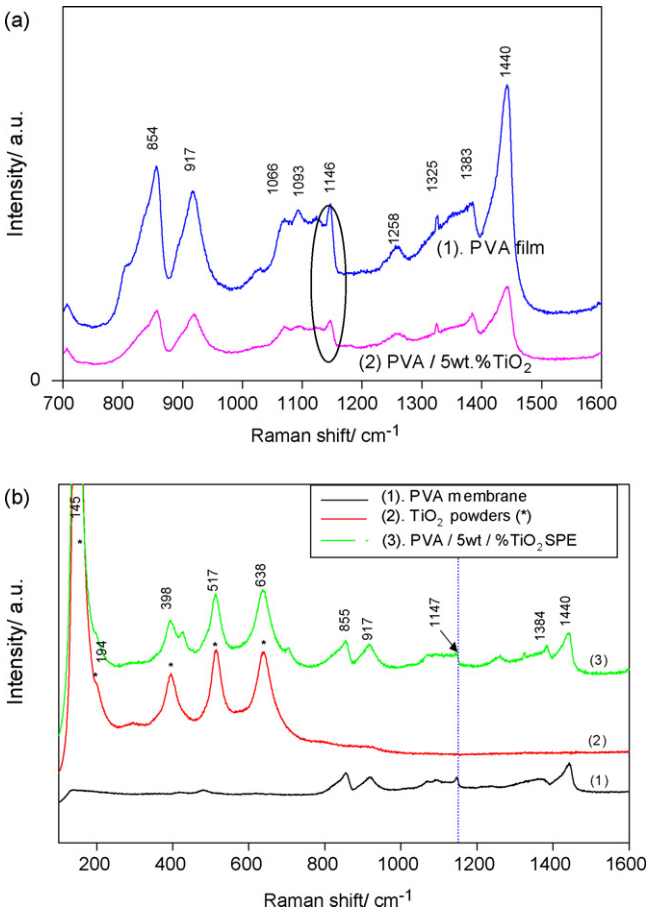

Fig. 3. Raman spectra for (a) PVA powders and film; (b) PVA film, TiO_2 powders and PVA/5 wt.% TiO_2 SPE.

Most importantly, it shows that the intensities of these Raman characteristic vibrational peaks of PVA/TiO_2 composite polymer membranes were greatly decreased; in particular, the vibrational peak at 1146 cm^{-1} was an indicator for the degree of crystallinity of the PVA polymer [34]. In other words, it also demonstrates that the amorphous regions in the PVA/TiO_2 composite polymer membrane increased greatly.

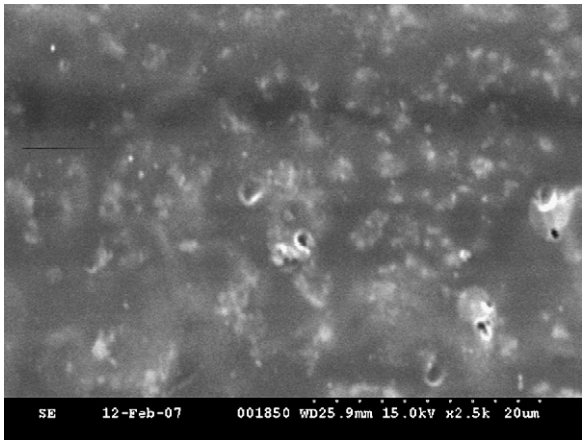

Fig. 2. SEM photographs for the PVA/5 wt.% TiO_2 composite polymer membrane at 2500×.

Table 1
Assignments for major Raman characteristic peaks of PVA polymer and TiO_2 powders

Frequency (cm^{-1})	Assignment
PVA polymer	
854	C–C stretch vibration
917	C–C stretch vibration
1066	C–O stretch, O–H bend vibration
1093	C–O stretch, O–H bend vibration
1146	C–O stretch, C–C stretch vibration
1383	C–H bend, O–H bend vibration
1440	C–H bend, O–H bend vibration
Nano-TiO_2 powders	
145	O–Ti–O bending-type vibration
194	O–Ti–O bending-type vibration
398	O–Ti–O bending-type vibration
517	Ti–O axial stretch vibration
638	Ti–O equatorial stretch vibration

3.3. Ionic conductivity and alcohol permeability measurements

The ionic conductivities of alkaline PVA/TiO_2 composite polymer electrolytes can be obtained using AC impedance analysis. All AC spectra are typically non-vertical spikes for stainless steel (SS) blocking electrodes, i.e., SS|PVA/TiO_2 SPE|SS cell (not shown). Analysis of the spectra yields information about the properties of the PVA/TiO_2 polymer electrolyte, such as bulk resistance, R_b. Taking into account the thickness of the composite electrolyte films, the R_b value was converted into the ionic conductivity value, σ, according to the equation: $\sigma = L/R_bA$, where L is the thickness (cm) of the PVA/TiO_2 composite polymer electrolyte, A is the area of the blocking electrode (cm^2), and R_b is the bulk resistance (Ω) of the alkaline composite polymer membrane.

Table 2 lists the ionic conductivity values of alkaline PVA/2.5–15 wt.% TiO_2 composite polymer membranes at different temperatures. The ionic conductivity value of alkaline PVA/2.5 wt.% TiO_2 composite polymer membranes was 0.0033 S cm^{-1} at 30 °C. Comparatively, the ionic conductivity values of alkaline PVA/TiO_2 composite polymer membranes with 5, 10 and 15 wt.% TiO_2 fillers were 0.0046, 0.0126 and 0.0480 S cm^{-1} at 30 °C, respectively. It shows that the highest ionic conductivity value of an alkaline composite polymer membrane containing 4 M KOH was for 15 wt.% TiO_2 fillers, i.e., σ = 0.0480 S cm^{-1} at ambient temperature.

According to the ionic conductivity result, it is clear that the ionic conductivity of PVA/TiO_2 composite polymer membrane increased when the amount of TiO_2 ceramic fillers increased. As we know, when the TiO_2 ceramic filler used as a stiffer material was added to the PVA matrix, the swelling ratio of PVA polymer membranes was also reduced (data not shown). As expected, the thermal property, ionic conductivity and dimension stability (less swelling ratio) all improved.

Fig. 4(a) shows the calibration curve for the methanol permeation experiment. This calibration curve was used to estimate the permeated methanol concentration for the PVA/TiO_2 composite membrane. Fig. 4(b) shows the methanol concentration vs. time curve for the PVA/10 wt.% TiO_2 composite membrane using 20 wt.% CH_3OH aqueous solution. Similarly, permeability measurements for the PVA/10 wt.% TiO_2 composite membrane using ethanol and IPA were also carried out. All values of alcohol permeability for the PVA/TiO_2 composite membranes were obtained from the slope of the straight line. The methanol, ethanol, and IPA permeability values of the PVA/TiO_2 composite membrane were 3.66×10^{-7}, 2.81×10^{-7}, and 5.09×10^{-8} cm^2 s^{-1}, respectively. Thus, IPA had the lowest value of permeability, while the methanol showed the highest value of permeability. However, the permeability value of the PVA/TiO_2 composite membrane (in the order of 10^{-7} to 10^{-8} cm^2 s^{-1}) was much lower than that of Nafion polymer membrane (in the order of 10^{-6} cm^2 s^{-1}) [5,34,35].

Table 2
The ionic conductivities of the PVA/TiO_2 composite polymer membranes with different contents of TiO_2 fillers at different temperatures

T (°C)	σ (S cm^{-1}); weight percent of TiO_2 fillers			
	2 wt.%	5 wt.%	10 wt.%	15 wt.%
30	0.0033	0.0046	0.0126	0.0480
40	0.0044	0.0071	0.0187	0.0541
50	0.0052	0.0111	0.0210	0.0670
60	0.0064	0.0166	0.0301	0.0812
70	0.0113	0.0230	0.0414	0.0901

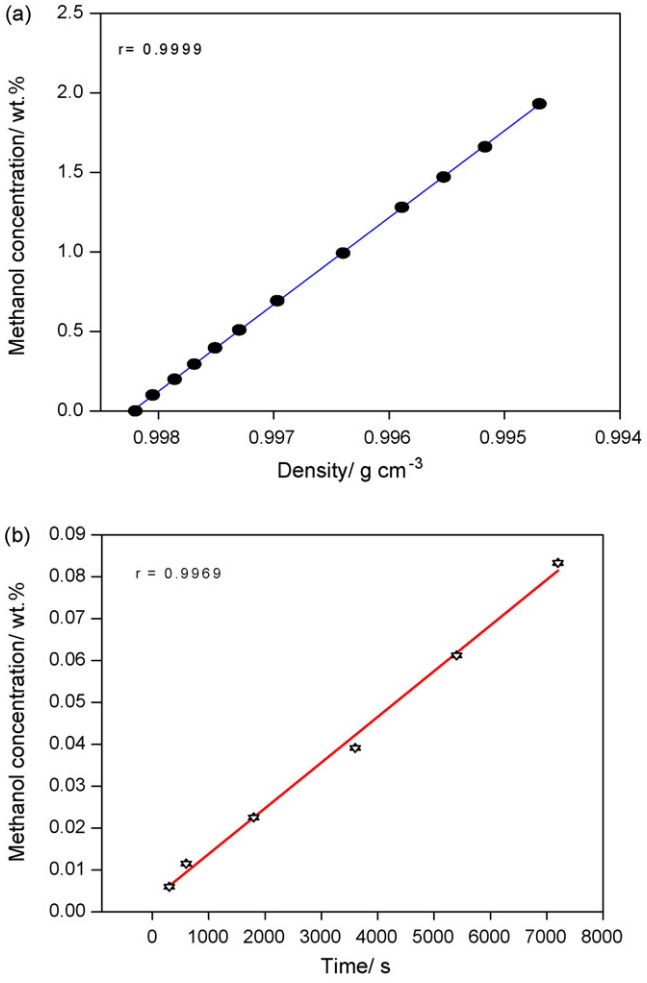

Fig. 4. The methanol permeability experiment: (a) the calibration curve; (b) the methanol concentration vs. time curve for the PVA/10 wt.% TiO_2 composite SPE.

3.4. Electrochemical measurements

The polarization curves for the air cathode (based on MnO_2/C) wrapping with a layer of PVA/10 wt.% TiO_2 composite polymer membrane in 4 M KOH and 4 M KOH + 2 M CH_3OH aqueous solutions, respectively, are shown in Fig. 5. The inset of Fig. 5 shows the Tafel plot for ORR on the air cathode with a Tafel slope of 230 mV dec^{-1}. It is apparent that the reduction current density (oxygen reduction reaction, ORR) for the air electrode in the 4 K KOH solution was higher than that for the air electrode in the 4 M KOH + 2 M CH_3OH solution. It is clear that the methanol crossover occurred through the PVA/TiO_2 composite polymer membrane and the crossover reduced the electroactivity of the air electrode, i.e., the methanol tended to block some active surface areas of the MnO_2 catalysts. As listed in Table 3, the degradation percentages of the air electrode, in terms of the current density, in the electrode potential range of 1.0–0.40 V (vs. RHE) were estimated at approximately ca. 2–7%. The higher the current density, the higher the alcohol crossover occurred. The ethanol and IPA crossover phenomena were also found for the air electrode (not shown). However, the extent of the degradation was less intense. It is well known that the MnO_2 cathode exhibits a much more tolerant alcohol crossover than the Pt electrode [39]. In fact, the I–V polarization results show that the alcohols crossover strongly affected the electrochemical performance of the air electrode. In addition, the degradation of the air electrode proved to be highly dependent on the types of

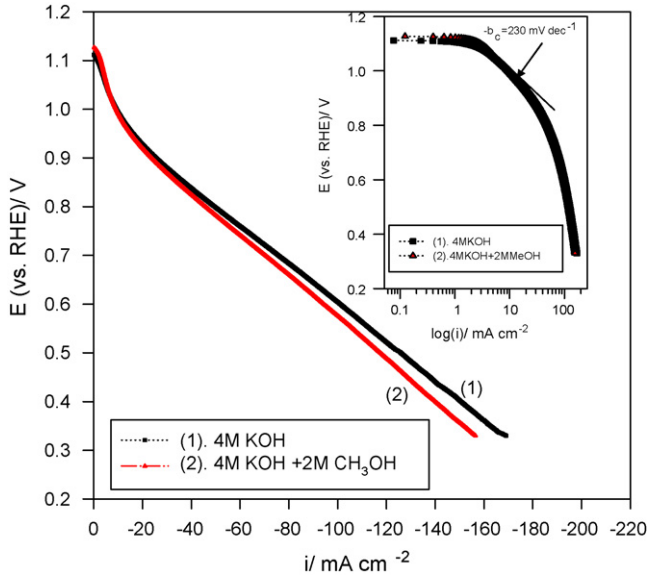

Fig. 5. The *I–V* curve for the air cathode wrapped with a layer of PVA/10 wt.% TiO_2 composite polymer membrane in 4 M KOH and 4 M KOH + 2 M CH_3OH solutions, respectively at ambient conditions.

Table 3
The results of *I–V* analyses for the air electrode wrapped with the PVA/10 wt.% TiO_2 composite polymer membrane in 4 M KOH and 4 M KOH + 2 M CH_3OH solutions

E (V)[a]	*i* (mA cm^{-2})		
	4 M KOH	4 M KOH + 2 M CH_3OH	Methanol crossover loss (%)
1.00	−9.24	−9.05	2.05
0.90	−25.49	−23.69	7.06
0.80	−49.28	−45.65	7.36
0.70	−75.53	−70.25	6.99
0.60	−100.98	−94.27	6.64
0.50	−125.73	−117.28	6.72
0.40	−150.39	−139.95	6.94

[a] Electrode potential (vs. RHE).

alcohol fuels employed, in terms of the polymer membranes and the cathode catalysts used.

The polarization curves for the anode containing 3.6 mg cm^{-2} PtRu black in various 4 M KOH + 2 M alcohols aqueous solutions at 25 °C are shown in Fig. 6. The results indicate that methanol showed the best electrochemical performance, while IPA was the poorest. The performance of the electrochemical alcohol oxidation sequence was as follows: methanol > ethanol > IPA.

Fig. 7 also displays the AC spectra for the PtRu anode in 4 M KOH + 2 M alcohols aqueous solutions at OCP. Apparently, the methanol electro-oxidation roved to be most favorable with the smallest impedance, while the IPA had the highest one.

Fig. 8 shows the *E–t* curves for alkaline DAFCs consisting of the PtRu anode, the MnO_2 cathode, and the PVA/10 wt.% TiO_2 composite polymer membrane in 4 M KOH + 2 M methanol, ethanol and IPA solutions, respectively, at 20 mA cm^{-2} at room temperature and

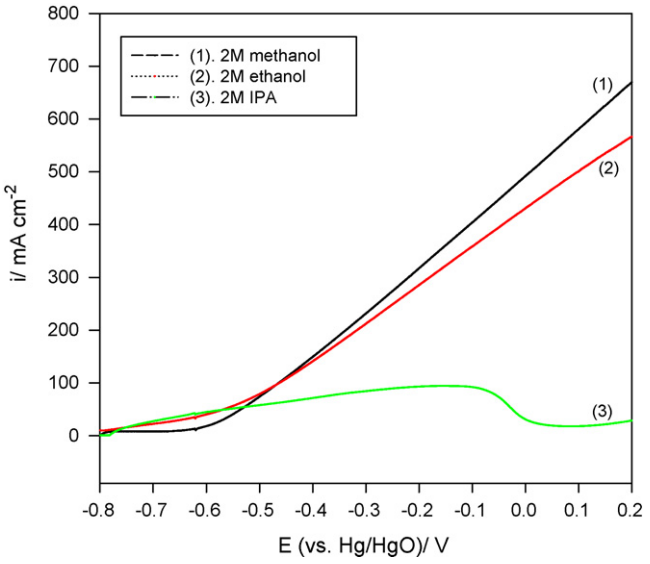

Fig. 6. The polarization curves for the PtRu anode in 4 M KOH + 2 M alcohol solutions.

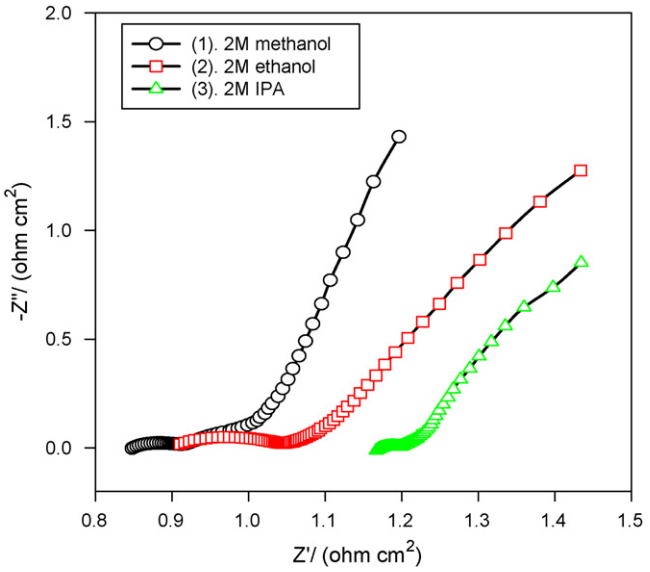

Fig. 7. AC spectra for the PtRu anode in 4 M KOH + 2 M alcohols at OCP.

ambient air. The average cell potentials of the DAFCs employing 2 M methanol, ethanol, and IPA as the fuels were 0.383, 0.341, and 0.264 V, respectively. In spite of a tendency to drop at the beginning of the test, the cell potentials leveled and remained constant during the test; it was estimated that the cell potential decay rates (by linear regression) for these alkaline DAFCs were around 10^{-5} to 10^{-6} V min^{-1}, as listed in Table 4.

Fig. 9 shows the potential–current density and the power density–current density curves for alkaline DAFCs in 4 M KOH + 2 M

Table 4
The results of galvanostatic analyses for alkaline DAFC in various 4 M KOH + 2 M alcohols solutions at 20 mA cm^{-2} at ambient temperature and pressure

Parameters	Solutions		
	2 M methanol	2 M ethanol	2 M IPA
OCP (V)	0.810	0.853	0.775
E_{cell} (V)	0.383	0.341	0.264
Decay rate (V min^{-1})	-1.784×10^{-5}	-9.174×10^{-6}	-7.524×10^{-6}
Cell potential (V) (regression line)	$E = 0.388 - 1.784 \times 10^{-5} \times t$	$E = 0.343 - 9.174 \times 10^{-5} \times t$	$E = 0.265 - 7.524 \times 10^{-6} \times t$

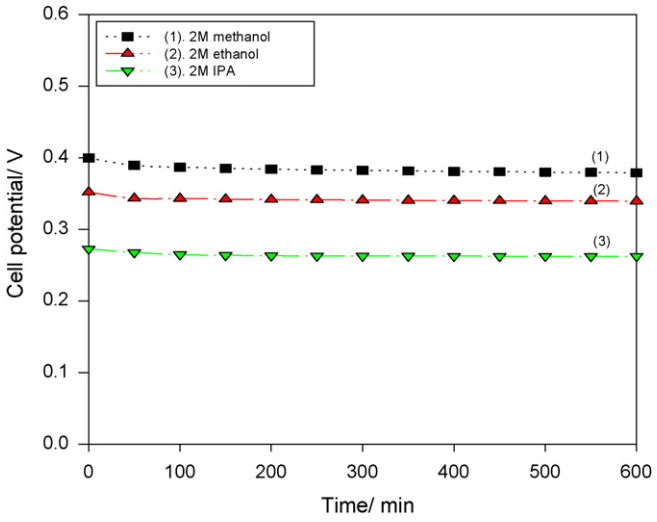

Fig. 8. The *E–t* curves for alkaline DAFCs comprising of the PVA/10 wt.% TiO_2 + GA SPE in 4 M KOH + 2 M alcohols at 20 mA cm^{-2}.

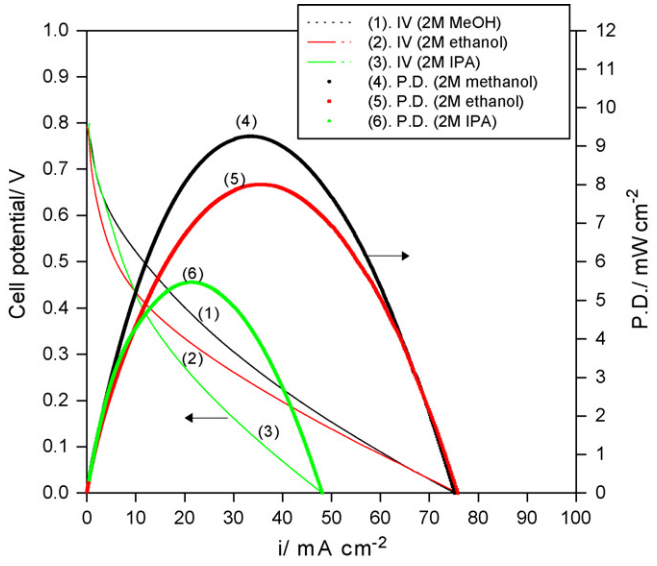

Fig. 9. The *I–V* and current density vs. P.D. curves for alkaline DAFCs comprising of the PVA/10 wt.% TiO_2 SPEs in 4 M KOH + 2 M alcohols solutions at 25 °C.

methanol, ethanol, and IPA solutions at room temperature, respectively. As a result, the maximum power density of 9.25 mW cm^{-2} for alkaline DAFC with 2 M methanol was achieved at $E_{p,max}$ = 0.276 V with a peak current density ($i_{p,max}$) of 33.57 mA cm^{-2}, as listed in Table 5. On the other hand, the maximum power density of alkaline DAFC with 2 M ethanol was 8.00 mW cm^{-2} at $E_{p,max}$ = 0.224 V with a peak current density of 35.68 mA cm^{-2} at 25 °C.

Furthermore, the maximum power density of alkaline DAFC with 2 M IPA was only 5.46 mW cm^{-2} at $E_{p,max}$ = 0.254 V with a peak current density of 21.46 mA cm^{-2} at 25 °C. As a result, the maximum peak power densities were also in the order of methanol > ethanol > IPA. Especially important was that methanol showed the highest power density (9.25 mW cm^{-2}) among the lower aliphatic alcohol fuels. The poor performance of the DAFC with 2 M IPA may have been due to the poor electrochemical activity for PtRu catalysts on the IPA.

Thus, these results suggest that the alkaline DMFC (methanol) system exhibited better performance as compared to that of the alkaline DEFC (ethanol) system. More importantly, the alkaline DAFC consists of an air electrode using a non-precious metal catalyst, i.e., a cheap MnO_2 catalyst instead of an expensive Pt. The metal oxide catalyst of MnO_2 is not only inexpensive but also more tolerant towards crossover, and is active during the reduction of O_2 to OH^- in alkaline media. Another advantage is that the PVA/TiO_2 composite polymer membrane is a cheap non-perfluorosulfonated polymer membrane, as compared to the expensive Nafion polymer membrane.

Table 5
The maximum peak power densities for alkaline DAFCs in 4 M KOH + 2 M alcohols solutions at ambient temperature and pressure

Parameters	Alcohols		
	2 M methanol	2 M ethanol	2 M IPA
P.D. (mW cm^{-2})	9.25	8.00	5.46
$i_{p,max}$ (mA cm^{-2})	33.57	35.68	21.46
$E_{p,max}$ (V)	0.276	0.224	0.254

4. Conclusions

The novel PVA/TiO_2 composite polymer membrane was successfully prepared using a solution casting method. Alkaline direct alcohol fuel cells (DAFCs) comprised of the PVA/TiO_2 composite polymer membrane were assembled and systematically examined. The DAFC was comprised of an air cathode based on MnO_2/C catalysts, a PtRu anode and PVA/TiO_2 composite polymer membrane. These DAFCs comprised of alkaline PVA/TiO_2 composite polymer membranes exhibited different electrochemical performances. Three lower aliphatic alcohol fuels (i.e., so-called C_1–C_3 alcohol), including methanol, ethanol, and IPA, were tested and compared. Among these alcohols, the maximum peak power density of the DAFC with 2 M methanol was about 9.25 mW cm^{-2}. Also, the maximum peak power densities were in the order methanol > ethanol > IPA.

The electrochemical performance of alkaline DAFC with methanol was somehow better than that of DAFC with ethanol, in terms of the maximum power density. However, the performance for the DAFC with 2 M IPA showed poor performance due to the poor electrochemical activity of the PtRu catalyst. A free-standing PVA/TiO_2 composite polymer membrane can easily be prepared. The PVA/TiO_2 composite polymer membrane is a potential candidate for application in terms of alkaline DAFC systems.

Acknowledgement

Financial support from the National Science Council, Taiwan (Project No: NSC-95-2221-E131-032) is gratefully acknowledged.

References

[1] W.H. Lizcano-Valbuena, V.A. Paganin, E.R. Gonzalez, Electrochim. Acta 47 (2002) 3715.
[2] N. Nakagawa, Y. Xiu, J. Power Sources 118 (2003) 248.
[3] G.G. Park, T.H. Yang, Y.G. Yoon, W.Y. Lee, C.S. Kim, Int. J. Hydrogen Energy 28 (2003) 645.
[4] H. Fukunaga, T. Ishida, N. Teranishi, C. Arai, K. Yamada, Electrochim. Acta 49 (2004) 2123.
[5] V. Baglio, A.S. Arico, A.D. Blasi, V. Antonucci, P.L. Antonucci, S. Licoccia, E. Traversa, F.S. Fiory, Electrochim. Acta 50 (2005) 1241.
[6] T.C. Deivaraj, J.Y. Lee, J. Power Sources 142 (2005) 43.
[7] K. Furukawa, K. Okajima, M. Sudoh, J. Power Sources 139 (2005) 9.
[8] J.H. Choi, Y.M. Kim, J.S. Lee, K.Y. Cho, H.Y. Jung, J.K. Park, I.S. Park, Y.E. Sung, Solid State Ionics 176 (2005) 3031.
[9] V.S. Silva, S. Weisshaar, R. Reissner, B. Ruffmann, S. Vetter, A. Mendes, L.M. Madeira, S. Nunes, J. Power Sources 145 (2005) 485.
[10] B.E. Hayden, D.V. Malevich, D. Pletcher, Electrochem. Commun. 3 (2001) 395.
[11] E. Antolin, Mater. Chem. Phys. 78 (2003) 563.
[12] G.Q. Lu, C.Y. Wang, J. Power Sources 144 (2005) 141.

[13] C.Y. Yang, P. Yang, J. Power Sources 123 (2003) 37.
[14] T. Shimizu, T. Momma, M. Mohamedi, T. Osaka, S. Sarangapani, J. Power Sources 137 (2004) 277.
[15] K. Kordesch, V. Hacker, U. Bachhiesl, J. Power Sources 96 (2001) 200.
[16] J.G. Liu, T.S. Zhao, R. Chen, C.W. Wong, Electrochem. Commun. 7 (2005) 288.
[17] B.K. Kho, I.H. Oh, S.A. Hong, H.Y. Ha, Electrochim. Acta 50 (2004) 781.
[18] F. Vigier, C. Coutanceau, F. Hahn, E.M. Belgsir, C. Lamy, J. Electroanal. Chem. 563 (2004) 81.
[19] E.V. Spinace, A.O. Neto, M. Linardi, J. Power Sources 129 (2004) 121.
[20] W.L. Zhou, S.Q. Song, W.Z. Li, G.Q. Sun, Q. Xin, S. Kontou, K. Poulianitis, P. Tsiakaras, Solid State Ionics 175 (2004) 797.
[21] Z. Liu, X.Y. Ling, X. Su, J.Y. Lee, L.M. Gan, J. Power Sources 149 (2005) 1.
[22] G.A. Camara, R.B.D. Lima, T. Iwasita, Electrochem. Commun. 6 (2004) 812.
[23] E.V. Spinace, M. Linardi, A.O. Neto, Electrochem. Commun. 7 (2005) 365.
[24] S.Q. Song, W.J. Zhou, Z.H. Zhou, L.H. Jiang, G.Q. Sun, Q. Xin, V. Leontidis, S. Kontou, P. Tsiakaras, Int. J. Hydrogen Energy 30 (2005) 995.
[25] X. Tang, B. Zhang, Y. Li, Y. Xu, Q. Xin, W. Shen, J. Mol. Catal. A: Chem. 235 (2005) 122.
[26] J.M. Leger, S. Rousseau, C. Coutanceau, F. Hahn, C. Lamy, Electrochim. Acta 50 (2005) 5118.
[27] W.J. Zhou, W.Z. Li, S.Q. Song, Z.H. Zhou, L.H. Jiang, G.Q. Sun, Q. Xin, K. Kontou, P. Tsiakaras, J. Power Sources 131 (2004) 217.
[28] M.R. Tarasevich, Z.R. Karichev, V.A. Bogdanovskaya, E.N. Lubnin, A.V. Kapustin, Electrochem. Commun. 7 (2005) 141.
[29] Y. Bai, J. Wu, J. Xi, J. Wang, W. Zhu, L. Chen, X. Qiu, Electrochem. Commun. 7 (2005) 1087.
[30] C. Xu, P.K. Shen, X. Ji, R. Zeng, Y. Liu, Electrochem. Commun. 7 (2005) 1305.
[31] C.C. Yang, J. Membr. Sci. 288 (2007) 51.
[32] C.C. Yang, S.J. Chiu, W.C. Chien, J. Power Sources 162 (2006) 21.
[33] Y. Wang, L. Li, L. Hu, L. Zhuang, J. Lu, B. Xu, Electrochem. Commun. 5 (2003) 662.
[34] S. Panero, P. Fiorenza, M.A. Navarra, J. Romanowska, B. Scrosati, J. Electrochem. Soc. 152 (12) (2005) A2400.
[35] H.Y. Chang, C.W. Lin, J. Membr. Sci. 218 (2003) 295.
[36] B. Bae, D. Kim, J. Membr. Sci. 220 (2003) 75.
[37] J. Kim, B. Kim, B. Jung, J. Membr. Sci. 207 (2002) 129.
[38] C.C. Yang, S.T. Hsu, W.C. Chien, M.C. Shih, S.J. Chiu, K.T. Lee, C.L. Wang, Int. J. Hydrogen Energy 31 (2006) 2076.
[39] A. Verma, A.K. Jha, S. Basu, J. Power Sources 141 (2005) 30.